

LETTER TO THE EDITOR

Plasma Mixing in Collisionless Kelvin–Helmholtz Dynamics

Silvia Ferro^{1,*}, Fabio Bacchini^{1,2}, Giuseppe Arrò³, Francesco Pucci⁴, and Pierre Henri^{5,6}

¹ Centre for mathematical Plasma Astrophysics, Department of Mathematics, KU Leuven, Celestijnenlaan 200B, B-3001 Leuven, Belgium

² Royal Belgian Institute for Space Aeronomy, Solar-Terrestrial Centre of Excellence, Ringlaan 3, 1180 Uccle, Belgium

³ Department of Physics, University of Wisconsin-Madison, Madison, WI 53706, USA

⁴ Institute for Plasma Science and Technology, National Research Council, CNR-ISTP, Bari, Italy

⁵ Laboratoire Lagrange, Observatoire Côte d’Azur, Université Côte d’Azur, CNRS, Nice, France

⁶ LPC2E, CNRS, Université d’Orléans, CNES, Orléans, France

February 20, 2026

ABSTRACT

Context. Simulations and observations of the low-latitude magnetosphere–magnetosheath boundary layer indicate that the Kelvin–Helmholtz instability (KHI) drives vortex structures that enhance plasma mixing and magnetic reconnection, influencing transport and particle acceleration.

Aims. We investigate the efficiency and physical mechanisms of plasma mixing driven by the nonlinear evolution of the KHI.

Methods. We perform high-resolution two-dimensional Particle-In-Cell (PIC) simulations using a finite-Larmor-radius shear-flow initial configuration. Plasma mixing is quantified using particle tracking, passive tracers, and diagnostics of magnetic reconnection.

Results. Mixing across the shear layer is present but localized, occurring mainly in narrow interface regions and plasma structures. Ions mix more effectively than electrons, which remain largely frozen to field lines. Enhanced mixing correlates with localized reconnection within and between KH vortices.

Conclusions. Cross-boundary transport driven by the kinetic KHI is highly localized and mediated by vortex advection and reconnection. Electron mixing is strongly constrained, providing an upper bound on kinetic-scale transport across collisionless shear layers.

Key words. KHI – plasma mixing – fully kinetic simulations

1. Introduction

The Kelvin–Helmholtz instability (KHI) develops when a plasma shear flow becomes super-Alfvénic with respect to the magnetic-field component parallel to the shear (Chandrasekhar 1961). At Earth’s low-latitude magnetopause, this condition is frequently met during intervals of strongly northward or southward interplanetary magnetic field (IMF), and signatures of surface waves and rolled-up vortices have been widely observed (Hasegawa et al. 2004; Eriksson et al. 2016; Stawarz et al. 2016; Settino et al. 2024). KH activity has also been reported at other planetary magnetospheres, including Mercury (Aizawa et al. 2020), Mars (Koh et al. 2025), Saturn (Dialynas 2018), and Jupiter (Montgomery et al. 2023), raising the question of how magnetospheric size influences the multi-scale development of the instability. After saturation, KH vortices generate strong gradients in velocity, density, and magnetic field down to ion and electron scales, triggering secondary instabilities that broaden the mixing layer and enhance plasma transport across the solar wind–magnetosphere boundary (Nykyri & Otto 2001; Hasegawa et al. 2004; Nakamura et al. 2017). Kinetic studies and in-situ observations show that this transport is mediated by processes such as reconnection, wave–particle interactions, and vortex-induced reconnection (VIR), enabling solar-wind plasma entry even under northward IMF conditions (Nykyri et al. 2006; Stawarz et al. 2016; Nakamura et al. 2017; Nakamura et al. 2020). While magnetohydrodynamic (MHD) simulations cap-

ture the global KH dynamics and reconnection-driven transport (Faganello et al. 2012; Ma et al. 2017; Ferro et al. 2024), they do not resolve the kinetic mechanisms governing particle diffusion and heating. Despite these advances, quantitatively characterizing plasma mixing in fully kinetic KHI remains challenging, particularly in distinguishing genuine plasma interpenetration from large-scale advection (Nakamura et al. 2013; Karimabadi et al. 2013).

In this Letter, we investigate plasma mixing driven by the nonlinear evolution of the collisionless KHI using fully kinetic Particle-in-Cell (PIC) simulations of an electron–ion plasma. We quantify mixing efficiency based on particle origin and kinetic diagnostics, and discuss the implications for solar wind–magnetosphere interactions.

2. Methodology and Simulation Setup

We perform 2D (PIC) simulations using semi-implicit methods (the Implicit Moment Method and the Energy Conserving Semi-Implicit Method) implemented in the iPIC3D and EC-sim codes (Markidis et al. 2010; Lapenta 2017; Bacchini 2023; Croonen et al. 2024). Details of the numerical methods are given in Appendix A.

We model a collisionless magnetized plasma with uniform per-species density n_0 and an initial magnetic field composed of an in-plane component along x and a guide field $B_{z,0} = 10B_{x,0}$. All quantities are normalized using ion reference scales: the ion gyro-frequency $\Omega_{c,i} = q_i B_{\text{tot},0} / (m_i c)$, where $B_{\text{tot},0} = \sqrt{B_{x,0}^2 + B_{z,0}^2}$

* silvia.ferro@kuleuven.be

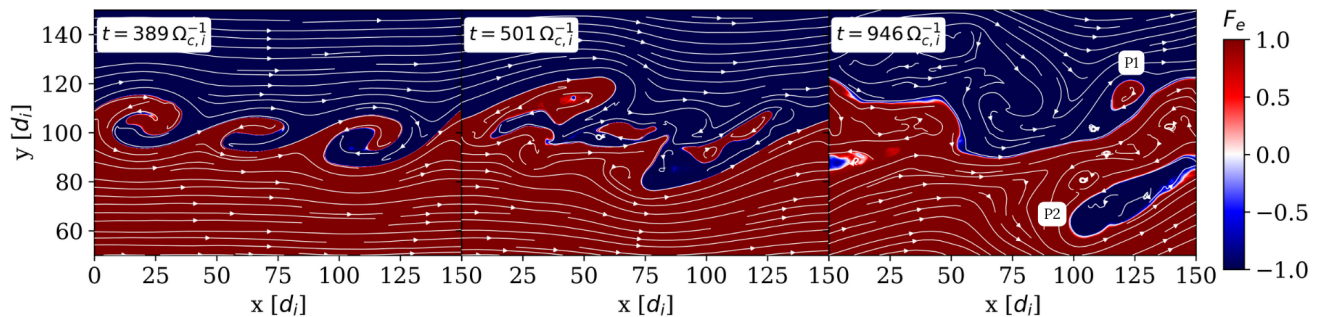


Fig. 1. From left to right: electron mixing fraction F_e in the lower shear layer during the nonlinear phase. Shown are the rolled-up vortices at $t = 389 \Omega_{ci}^{-1}$, their merging at $t = 501 \Omega_{ci}^{-1}$, and the late nonlinear stage at $t = 946 \Omega_{ci}^{-1}$. White lines trace the in-plane magnetic field; in the right panel, two ejected plasma parcels (P1: red; P2: blue) are highlighted.

is the total magnetic field magnitude at initialization; the ion plasma frequency $\omega_{p,i} = (4\pi n_0 q_i^2 / m_i)^{1/2}$; the ion inertial length $d_i = c / \omega_{p,i}$; and the Alfvén speed $v_A = B_{\text{tot},0} / \sqrt{4\pi n_0 m_i}$. At initialization, the ion cyclotron-to-plasma frequency ratio is $\Omega_{ci} / \omega_{p,i} = 0.05$.

The initial equilibrium configuration is implemented following the approach of Cerri et al. (2013), ensuring a self-consistent shear-velocity profile within a finite-Larmor-radius (FLR) framework. Although this is not an exact kinetic equilibrium, it retains first-order FLR corrections, which significantly reduce the spurious fluctuations that arise from pressure-tensor responses at ion kinetic scales when using fluid-like MHD initial conditions, thereby yielding a more accurate representation of shear layers only a few ion Larmor-radii thick (Henri et al. 2013). Ions and electrons are initialized with drifting Maxwellian distributions with an initial drift velocity $V_{\text{drift}} = 0.28 c$. Our boundary conditions are periodic in all directions. We impose an initial velocity profile with a double shear

$$V_x(y) = V_{\text{drift}} \left[\tanh\left(\frac{y - y_{sh,1}}{\delta}\right) - \tanh\left(\frac{y - y_{sh,2}}{\delta}\right) - 1 \right], \quad (1)$$

where $\delta = 3d_i$ represents the initial shear-layer thickness, and the shears are located at $y_{sh,1} = L_y/4$ and $y_{sh,2} = 3L_y/4$. The shear layers are chosen to study configurations where vorticity and guide magnetic field are parallel (at $y_{sh,1}$) or anti-parallel (at $y_{sh,2}$). The computational domain is a 2D box of size $150d_i \times 400d_i$ with 2304×6144 grid points, giving a spatial resolution $\Delta x = 0.0651 d_i = 0.5208 d_e = 5.21 \lambda_D$ with $\lambda_D = v_{th,e} / \omega_{p,e}$ the Debye length. The time step is $\Delta t = 0.1 \omega_{p,i}^{-1}$. This choice resolves the electron gyration with approximately 17.6 time steps per cyclotron rotation. The ion-to-electron mass ratio is $m_i/m_e = 64$, with 640 particles per cell. The temperature ratio is $T_e/T_i = 0.2$, and the plasma- $\beta = n_0 kT / (B_0^2 / (8\pi))$ for ions and electrons is $\beta_i = 0.5$ and $\beta_e = 0.1$, respectively. The most unstable KH mode has a wavelength of $L_x/3$, leading to the formation of three vortices in each shear layer as the system enters the nonlinear phase. We identify four distinct stages in the evolution: a linear phase ($t = 0-250, \Omega_{ci}^{-1}$) with exponential growth, an early nonlinear phase ($t = 250-450, \Omega_{ci}^{-1}$), a merging phase ($t = 450-650, \Omega_{ci}^{-1}$) dominated by vortex coalescence, and a late nonlinear phase ($t > 650, \Omega_{ci}^{-1}$) characterized by increasingly turbulent behavior. In this study, we focus on the nonlinear evolution, including the early, merging, and late nonlinear phases. Plasma mixing is tracked by assigning each particle a label ℓ based on its initial y -position, with $\ell = 0$ for particles initialized in $y < y_{sh,1}$ or $y > y_{sh,2}$, and $\ell = 1$ for those initialized in $y_{sh,1} < y < y_{sh,2}$. This labeling allows us to distinguish particles

originating from different regions and to track their movement across shear layers, providing a measure of plasma transport and mixing for both ions and electrons.

3. Plasma Mixing and Magnetic Reconnection

In Figure 1, we show snapshots representative of the evolution of the vortices at the lower shear during the nonlinear stage of the KHI. The quantity shown is the electron mixing fraction (Nakamura & Daughton 2014), $F_e = (n_{e,\ell=1} - n_{e,\ell=0}) / n_e$, where $n_{e,\ell=1}$ and $n_{e,\ell=0}$ are the electron number densities initially on either side of the shear. Regions with $F_e = -1$, $F_e = 1$, and $|F_e| < 1$ correspond to unmixed plasma on either side and mixed plasma, respectively. The ion mixing fraction and the upper shear layer for both species behave similarly and are not shown.

The left panel of Figure 1 shows three rolled-up vortices at the early nonlinear stage. As they merge (middle panel), a dynamic *mixing layer* forms, where plasma parcels can temporarily cross regions before returning to their origin (Figure 1, middle and left panels). Magnetic tension limits permanent cross-field transport: although reconnection allows plasma parcels to detach from their original field lines, the strong in-plane field pulls them back. Consequently, magnetic tension counteracts plasma transport and forces macroscopic parcels to rebound toward their region of origin, limiting their ability to permanently migrate into the opposite region. Appendix B further illustrates how the in-plane field constrains KHI-driven mixing.

While the mixing fraction provides the qualitative picture described above, it does not allow us to adequately quantify actual mixing because it does not capture the movement of small groups of particles potentially crossing between regions. To quantify interpenetration more accurately, we use a new tracer \tilde{n} based on the labeling scheme described in section 2. For each particle species, it is defined as the absolute change in particle density on either side of the shear:

$$\tilde{n}(x, t) = \sum_{\ell} |n_{\ell}(x, t) - n_{\ell}(x, t = 0)|, \quad (2)$$

summing over all labeled populations. This highlights regions where plasma from different initial regions mixes, providing a clearer visualization than the mixing fraction. In essence, this tracer identifies any cell of the domain in which particles with a certain label ℓ (belonging to a specific side of the shear at $t = 0$) are present at time t . In regions where particles with a certain ℓ were not initially present, the tracer assumes a value > 0 .

In Figure 2, we compare the spatial distribution of \tilde{n}/n_0 around both shear layers at different stages of the KHI for ions

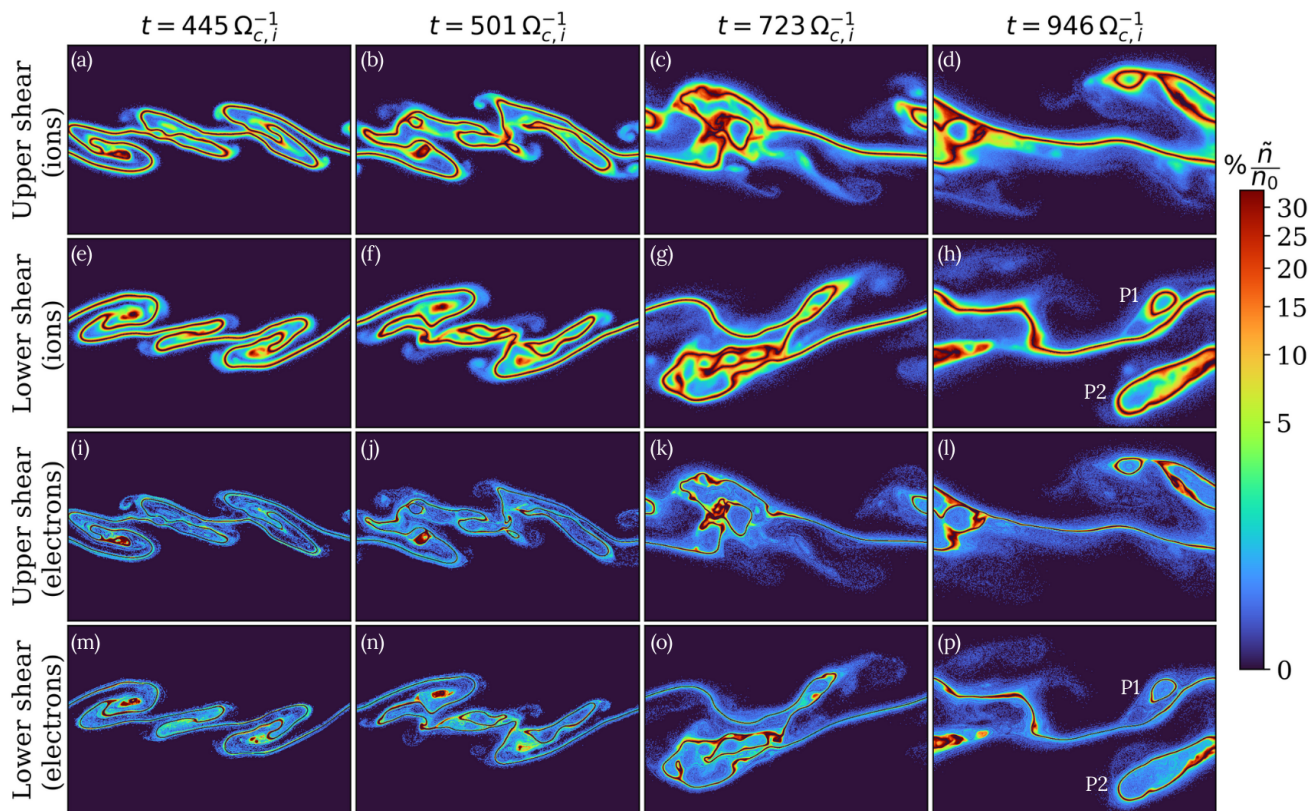


Fig. 2. Morphological evolution of the lower ($y = y_{sh,1}$) and upper ($y = y_{sh,2}$) shear layers at $t = 445, 501, 723, 946 \Omega_{c,i}^{-1}$ during the nonlinear stage of the KHI. Each panel shows a region around each shear that is $100 \times 150 d_i^2$. The colorbar shows \tilde{n}/n_0 in percentage, which describes the mixing of the two plasma regions normalized to the initial value (see text). The top two rows show the ion mixing (a–d upper shear, e–h lower shear), and the bottom two rows show the electron mixing (i–l upper shear, m–p lower shear).

and electrons. In the top two rows, we observe that ions mix more efficiently both close to and farther away from the frontier. In the bottom two rows, we observe that electrons mix less efficiently, especially at early times. At later stages, there are localized regions around plasma parcels and the frontier where the electron and ion mixing level increases, reaching values up to 30%. These peaks are very localized, and in general, plasma mixing remains only mildly efficient, with most particles penetrating the opposite plasma region only marginally. For ions, higher mixing levels are observed, particularly within plasma parcels that have fully crossed from one region to the other. In the right panel of Figure 1, two such parcels, P1 and P2, are highlighted and also shown in panels (h) and (p) of Figure 2, exhibiting higher internal mixing, particularly for ions in (h). This suggests that while plasma elements are advected coherently by the KH dynamics, intra-parcel diffusion promotes additional mixing. Other regions farther away from the frontier also show elevated mixing (see all panels in Figure 2 at times $t = 723, 946 \Omega_{c,i}^{-1}$).

To quantify plasma mixing, we compute the volume-averaged \tilde{n}/n_0 within the $100 \times 150 d_i^2$ regions highlighted in Figure 2. The left panel of Figure 3 shows its temporal evolution in both shear layers during the nonlinear phase. Although mixing can locally reach 30%, its strong localization keeps the volume-averaged fraction low. Ions cross the interface more efficiently than electrons, reaching averages of $\sim 7\%$ compared to $\sim 3\%$ for electrons. Around $t \simeq 300 \Omega_{c,i}^{-1}$, when fully rolled-up vortices form, mixing increases for both species, especially ions, then plateaus after $t \simeq 850 \Omega_{c,i}^{-1}$. As Figure 2 shows, low average

mixing is expected, since mixing mostly occurs near the interface and within plasma parcels crossing it coherently. We also show here that mixing is similar for different layers, implying that anti-alignment between vorticity and magnetic field plays no evident role in this dynamics.

To understand the link between magnetic-field dynamics and mixing, we analyzed magnetic-reconnection activity by measuring the out-of-plane current density and X-point formation at the shear layers. The middle panel of Figure 3 shows the temporal evolution of the maximum out-of-plane current density J_z for each species and shear layer. In our 2D geometry, the reversal of the in-plane magnetic field is sustained by a J_z sharply localized at X-points, making it an effective proxy for magnetic reconnection. J_z evolves similarly in both shears, with electron currents generally larger in magnitude, as expected from the mass difference between species. For $t \gtrsim 200 \Omega_{c,i}^{-1}$, the current density begins to increase in both species, reaching saturation around $t \simeq 400 \Omega_{c,i}^{-1}$. This coincides with the onset of the early nonlinear KHI and the beginning of the vortex-merging stage (left and middle panels of Figure 1), as well as the previously noted rise in the mixing percentage. The right panel of Figure 3 shows the number of X-points over time at each shear layer. X- and O-points are identified as nulls of the magnetic-flux gradient, $\nabla\psi = \mathbf{0}$, and distinguished by the sign of the Hessian determinant, following standard 2D reconnection diagnostics (Servidio et al. 2009; Wan et al. 2013; Olshevsky et al. 2016). The X-point count increases from $t \gtrsim 300 \Omega_{c,i}^{-1}$, corresponding to the early nonlinear stage of the KHI. These diagnostics indicate that enhanced reconnection activity—higher $\max |J_z|$ and more

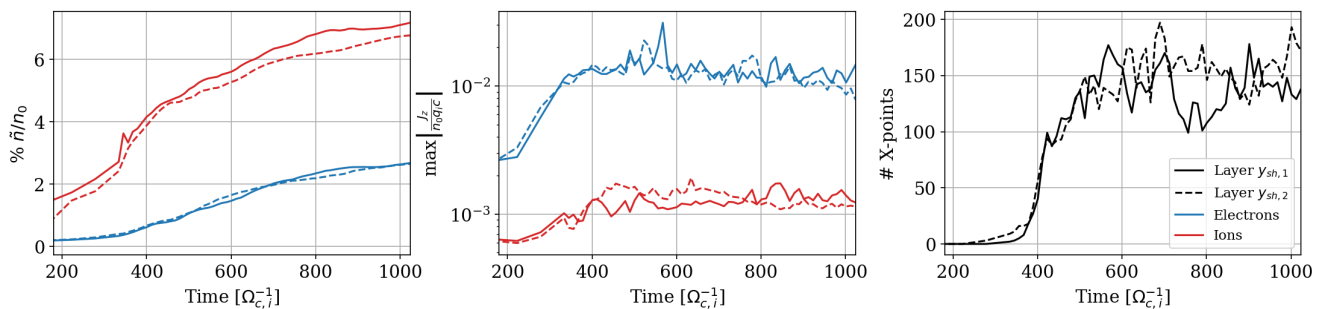


Fig. 3. Temporal evolution of plasma mixing, current density, and X-points. Bottom and top shear layers ($y_{sh,1}$, solid; $y_{sh,2}$, dashed) are indicated in all panels. Left panel: percentage of mixed plasma \tilde{n}/n_0 for electrons (blue) and ions (red). Middle panel: maximum absolute out-of-plane current density $|J_z|/(n_0 q_i c)$ for electrons (blue) and ions (red). Right panel: number of X-points in each shear layer.

X-points—coincides with increased plasma mixing (\tilde{n}/n_0). As reconnection breaks and reconnects field lines, particles from opposite sides of the shear are transported along newly connected lines, promoting cross-field mixing in frontier regions and detached plasma parcels.

4. Conclusions

We investigated the efficiency of plasma mixing driven by the nonlinear development of the magnetized KHI using high-resolution 2D fully kinetic simulations with finite-Larmor-radius effects (Cerri et al. 2013) and diagnostics including particle tracking, a new mixing tracer, and reconnection proxies. They show that, in this setup, mixing between magnetosheath and magnetospheric plasmas is present but relatively inefficient, even after KH vortices form and the nonlinear stage develops. Mixing is highly localized, reaching 30% only in sparse locations within a narrow interface layer and isolated advected parcels, and is generally absent farther from the shear layers. On average, ions achieve somewhat higher mixing levels than electrons, whereas electron mixing remains weak and largely confined to localized structures. We can explain this behavior by considering that ions are significantly less magnetized than electrons, allowing them to partially cross the shear interface, whereas electrons remain tightly bound to field lines. With a reduced mass ratio ($m_i/m_e = 64$), the actual electron magnetization in physical plasmas would be even higher, and their mixing correspondingly lower, meaning that electron mixing here likely represents an upper bound. Enhanced mixing occurs mainly within plasma parcels that detach and reattach across the interface, suggesting a significant contribution from magnetic reconnection and individual particle dynamics. Regions located between the interface and these parcels exhibit intermittent increase in mixing, coinciding with enhanced magnetic reconnection signatures, such as elevated out-of-plane current and higher X-point counts. This correspondence suggests that reconnection may facilitate localized cross-field transport during the nonlinear development of the KHI.

While these results provide new insights into localized plasma transport during the nonlinear KHI, there are some limitations that should be noted. The simulations are 2D and use a reduced ion-to-electron mass ratio, which may overestimate electron mobility and limit the range of three-dimensional reconnection dynamics. Despite these limitations, this Letter provides clear, fully kinetic evidence that plasma mixing driven by the nonlinear KHI remains intrinsically localized and heavily influenced by in-plane components of the magnetic field. By introducing a new mixing parameter and combining it with

particle tracking and reconnection diagnostics, we identify the specific structures—detached plasma parcels and reconnection sites—where cross-field transport is enhanced. Future work could extend these studies to fully three-dimensional setups, explore realistic mass ratios, and have a more detailed investigation of reconnection physics at the particle level, which could further clarify its role in facilitating cross-field transport.

Acknowledgements. S.F. is supported by the FWO PhD fellowship "Investigating Magnetospheric Plasma Dynamics with Large-scale Fully Kinetic Simulations" (grant no. 1126325N). F.B. acknowledges support from the FED-TWIN programme (profile Prf-2020-004, project "ENERGY") issued by BELSPO, and from the FWO Junior Research Project G020224N granted by the Research Foundation – Flanders (FWO). The resources and services used in this work were provided by the VSC (Flemish Supercomputer Center), funded by the Research Foundation - Flanders (FWO) and the Flemish Government.

References

- Aizawa, S., Raines, J. M., Delcourt, D., Terada, N., & André, N. 2020, *J. Geophys. Res. Space Phys.*, 125, e27871
 Bacchini, F. 2023, *ApJS*, 268, 60
 Brackbill, J. U. & Forslund, D. L. 1982, *J. Comput. Phys.*, 46, 271
 Cerri, S. S., Henri, P., Califano, F., et al. 2013, *Phys. Plasmas*, 20, 112112
 Chandrasekhar, S. 1961, *Hydrodynamic and hydromagnetic stability*
 Croonen, J., Pezzini, L., Bacchini, F., & Lapenta, G. 2024, *ApJS*, 271, 63
 Dialynas, K. 2018, *J. Geophys. Res. Space Phys.*, 123, 7271
 Eriksson, S., Lavraud, B., Wilder, V., et al. 2016, *Geophys. Res. Lett.*, 43, 5606
 Faganello, M., Califano, F., Pegoraro, F., Andreussi, T., & Benkadda, S. 2012, *Plasma Phys. Control. Fusion*, 54, 124037
 Ferro, S., Faganello, M., Califano, F., & Bacchini, F. 2024, *Phys. Plasmas*, 31, 052902
 Hasegawa, H., Fujimoto, M., & Phan, T. D. 2004, *Nature*, 430, 755
 Henri, P., Cerri, S. S., Califano, F., et al. 2013, *Phys. Plasmas*, 20, 102118
 Karimabadi, H., Roytershteyn, V., Wan, M., et al. 2013, *Phys. Plasmas*, 20, 102118
 Koh, Z.-W., Poh, G., Fowler, C. M., et al. 2025, *Geophys. Res. Lett.*, 52, 102118
 Lapenta, G. 2017, *J. Comput. Phys.*, 334, 349
 Ma, X., Delamere, P., Otto, A., & Burkholder, B. 2017, *J. Geophys. Res. Space Phys.*, 122, 10382
 Markidis, S., Lapenta, G., & Rizwan-uddin. 2010, *Math. Comput. Simul.*, 80, 1509
 Montgomery, J., Ebert, R. W., Allegrini, F., et al. 2023, *Geophys. Res. Lett.*, 50, 102118
 Nakamura, T. K. M. & Daughton, W. 2014, *Geophys. Res. Lett.*, 41, 8704
 Nakamura, T. K. M., Daughton, W., Karimabadi, H., & Eriksson, S. 2013, *J. Geophys. Res. Space Phys.*, 118, 5742
 Nakamura, T. K. M., Eriksson, S., Hasegawa, H., et al. 2017, *J. Geophys. Res. Space Phys.*, 122, 11,505
 Nakamura, T. K. M., Hasegawa, H., Daughton, W., et al. 2017, *Nature Communications*, 8, 1582
 Nakamura, T. K. M., Plaschke, F., Hasegawa, H., et al. 2020, *Geophys. Res. Lett.*, 47, 102118
 Nykyri, K. & Otto, A. 2001, *Geophys. Res. Lett.*, 28, 3565
 Nykyri, K., Otto, A., Lavraud, B., et al. 2006, *Ann. Geophys.*, 24, 2619
 Olshevsky, V., Deca, J., Divin, A., et al. 2016, *Astrophys. J.*, 819, 52
 Servidio, S., Matthaeus, W. H., Shay, M. A., Cassak, P. A., & Dmitruk, P. 2009, *Phys. Rev. Lett.*, 102, 115003
 Settino, A., Nakamura, R., Blasl, K. A., et al. 2024, *J. Geophys. Res. Space Phys.*, 129, 102118
 Stawarz, J. E., Eriksson, S., Wilder, F. D., et al. 2016, *J. Geophys. Res. Space Phys.*, 121, 11,021
 Wan, M., Matthaeus, W. H., Servidio, S., & Oughton, S. 2013, *Phys. Plasmas*, 20, 042307

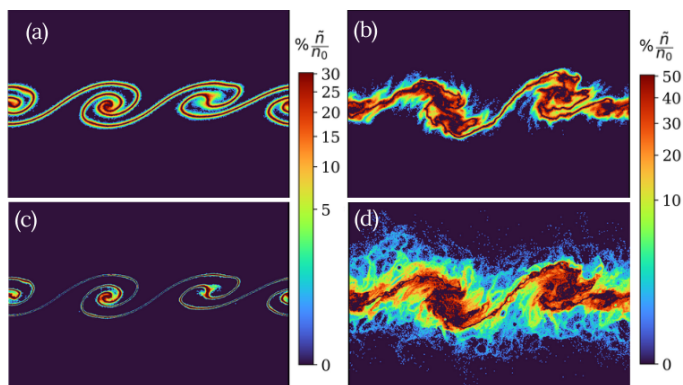


Fig. B.1. Panels (a) and (c) show the percentage of mixed plasma, \tilde{n}/n_0 , for ions and electrons in the lower shear layer with a finite B_x at $t = 334 \Omega_{ci}^{-1}$. Panels (b) and (d) show the corresponding ion and electron distributions in the lower shear layer without B_x at the same time. Each panel shows a region around the shear layer of size $100 \times 150 d_i^2$. A power-law normalization is used to enhance the visibility of low-amplitude structures.

Appendix A: Semi-Implicit PIC Methods

PIC codes typically use explicit time integration, which requires resolving the Debye length and the electron plasma frequency and is constrained by the Courant–Friedrichs–Lewy condition. Semi-implicit methods relax these constraints by linearizing or exactly treating the coupling between particles and fields, allowing simulations to retain small temporal and spatial scales, including electron-scale dynamics, while employing large domains. In this work, the first part of the simulation uses the Implicit Moment Method (IMM, Brackbill & Forslund 1982), which approximates the particle–field coupling and provides enhanced stability compared to explicit methods. The subsequent stage employs the Energy Conserving Semi-Implicit Method (ECSIM, Lapenta 2017). ECSIM replaces the nonlinear particle–field coupling with an exact relation, conserves energy exactly, retains the stability of fully implicit methods, and allows larger time steps and grid sizes while accurately capturing electron-scale dynamics.

The results shown in this Letter correspond to the nonlinear stage of the Kelvin–Helmholtz instability. We start the simulation with the IMM until the KHI develops, and then switch to ECSIM at the early stages of the nonlinear phase, so that all results presented here are obtained using ECSIM.

Appendix B: Effect of the In-plane Magnetic Field on Plasma Mixing

To further support the interpretation proposed in the main text, we compare in Figure B.1 the nonlinear evolution of the lower shear layer in simulations performed with and without an in-plane magnetic field B_x . These simulations employ the same physical and numerical setup as the reference run discussed in section 2, but with a spatial resolution reduced by a factor of four. Despite the reduced resolution, the simulations capture the large-scale nonlinear dynamics of the KHI and enable a clear assessment of the role of the in-plane magnetic field in regulating plasma mixing.

Panels (a) and (c) of Figure B.1 show the spatial distribution of the percentage of mixed plasma, \tilde{n}/n_0 , for ions and electrons, respectively, in the presence of a finite B_x . In this case, as KH vortices develop, plasma mixing remains weak and is largely

confined to the narrow interface between the two plasma regions. Although vortical structures form and advect plasma across the shear layer, the in-plane magnetic field limits cross-field transport, resulting in well-defined vortices and localized mixing (up to 30%) primarily concentrated near the frontier, in line with the discussion presented in the main text. In contrast, panels (b) and (d) show the corresponding ion and electron distributions, always for the lower shear in the absence of an in-plane magnetic field. In this case, the nonlinear evolution of the KHI is accompanied by significantly enhanced plasma mixing (up to 50%), with particles transported far from the initial interface and mixing regions extending well into both plasma domains. The absence of magnetic tension allows vortical motions to more efficiently redistribute plasma across the shear layer, leading to a broader and more spatially extended mixing region.

This comparison indicates that the limited and localized mixing observed in the main simulations is a robust physical effect associated with the presence of the in-plane magnetic field, rather than a consequence of numerical resolution. The in-plane field thus plays a key role in constraining cross-field transport and limiting the efficiency of plasma mixing in the nonlinear phase of the instability.